SUBMITTED MANUSCRIPT
INORGANIC CHEMISTRY

$ScRu_2B_3$ and Sc_2RuB_6, new borides featuring a 2D infinite boron clustering

L.P. Salamakha[1,4], O. Sologub[1,*], B. Stöger[2], P.F. Rogl[3], M. Waas[1], V. Kapustianyk[4], E. Bauer[1]

[1]Institute of Solid State Physics, TU Wien, A-1040 Vienna, Austria

[2]X-Ray Centre, TU Wien, A-1060 Vienna, Austria

[3]Institute of Materials Chemistry and Research, University of Vienna, A-1090 Vienna, Austria

[4]Department of Solid State Physics, Faculty of Physics, I. Franko L'viv National University, 79005, L'viv, Ukraine

ABSTRACT.

Two borides, $ScRu_2B_3$ and Sc_2RuB_6 were obtained by argon-arc melting of the elements followed by annealing at 800 ºC. $ScRu_2B_3$ exhibits a new structure type with the space group *Cmcm* (*a*=3.0195(2) Å, *b*=15.4056(8) Å, *c*=5.4492(3) Å; single crystal X-ray data; R_F^2=0.0105). Sc_2RuB_6 adopts the Y_2ReB_6-type structure (space group *Pbam*; *a*=8.8545(2) Å, *b*=11.1620(3) Å, *c*=3.4760(1) Å; single crystal X-ray data; R_F^2=0.0185). $ScRu_2B_3$ displays an unusual intergrowth of $CeCo_3B_2$- and AlB_2- related slabs; a striking feature is a boat configuration of puckered boron hexagons within infinite $B6^3$ nets. Sc_2RuB_6 presents two-dimensional planar nets of condensed boron pentagons, hexagons and heptagons sandwiched between metal layers. In Sc/Y substituted Y_2ReB_6-type, Y atoms are distributed exclusively inside the boron heptagons. Exploration of the Sc-Ru-B system at 800 ºC including binary boundaries employing EPMA and powder X-ray diffraction technique furthermore rules out the existence of previously reported "$ScRuB_4$" but confirms the formation and crystal structure of $Sc_2Ru_5B_4$. $ScRu_4B_4$ forms in cast alloys ($LuRu_4B_4$-type structure; space group $I4_1/acd$ (no. 142), *a*=7.3543(2) Å, *c*=14.92137(8) Å). Cell parameters and atomic coordinates have been refined for $ScRu_2B_3$, Sc_2RuB_6 and $ScRu_4B_4$ in the scope of generalized gradient approximation. Ab initio electronic structure calculations indicate a moderate electronic density of states at the Fermi level situated near the upper edge of essentially filled *d*-bands. Electrical resistivity measurements characterize $ScRu_2B_3$ and Sc_2RuB_6 as metals in concord with electronic band structure calculations.

Keywords: borides, crystal structure, electronic structure, X-ray diffraction, boron networks

INTRODUCTION

M-T-B systems (M=rare earth metal, Y, Sc, U, Th; T=Ru, Rh) attracted considerable interest owing to the interesting interplay between superconducting and magnetic properties of ternary phases and a large structural variety.[1-7] Perhaps, the most well known are the MRh_4B_4 compounds of $CeCo_4B_4$-type for which the T_C's range from *ca*. 2.5 K to 12 K for Sm and Lu compounds respectively[3]. Among the boride systems with Ru, $ScRu_4B_4$ ($LuRu_4B_4$-type) is most distinguished by a rather high superconducting transition temperature (*ca*. 7.2 K) in contrast to other members which are either not superconducting or order magnetically.[1] Superconductivity has been also observed in a number of $LuRuB_2$-type phases (M=Y, Lu; T=Ru,Os), among them the highest Tc (*ca*. 10 K) was found for $LuRuB_2$. The isotypic compounds with T=Tb - Tm order magnetically with critical temperatures in the range 2 K to 46 K.[8]

Despite the plentitude of interesting physical properties for M-T-B phases, some systems have only been studied scantily. An early report on the constitution of the Sc-Ru-B system employing powder X-ray diffraction and electron microprobe analysis identified three ternary phases existing in as cast conditions: $ScRu_4B_4$ ($LuRu_4B_4$-type structure, space group $I4_1/acd$, a=7.346 Å, c=14.895 Å), $ScRuB_4$ (unknown structure) and $ScRu_2B_2$ (unknown structure);[9] for the latter compound the single crystal X-ray data analysis led to the composition $Sc_2Ru_5B_4$ and revealed a monoclinic unit cell (space group $P2/m$, a=8.486 Å, b=3.0001 Å, c=9.983 Å, β=90.01°) for the sample annealed at 1000 ºC.[10] Information on the B-rich areas (≥50 at.% B) of related Sc-(Fe,Co,Ni,Rh,Os,Ir)-B systems is scarce as well. Compounds of two structure types were found to form at 66.6 at.% B: the $YCrB_4$-type and Y_2ReB_6-type phases in the Sc-Fe(Co,Ni)-B[11] and Sc-Rh(Ir)-B[12] systems, respectively. The structures exhibit two-dimensional boron planar nets composed of condensed boron polygons sandwiched between M/T layers. Decreasing contents of boron (to about 50 at.%) reduce the formation of boron-boron aggregates resulting in formation of boron ribbons, chains, pairs and isolated B atoms as encountered in $MgOs_3B_4$-, $LuRuB_2$- and $ZrIr_3B_4$-types compounds observed in Sc-Os(Ir)-B systems.[13-15]

Our interest in compounds exhibiting extensive boron atom clustering[12,16-18] inspired the study of the B-rich corner of the Sc-Ru-B system. In this context we report herein on the synthesis, structures and properties of two new ternary compounds, $ScRu_2B_3$ and Sc_2RuB_6. The structures of both compounds were determined by single crystal X-ray diffraction. $ScRu_2B_3$ represents a new type of boride structures and features an unusual intergrowth of

$CeCo_3B_2$-and AlB_2-related fragments. Sc_2RuB_6, which was observed for the first time, crystallizes with the Y_2ReB_6-type; examination of atom site distribution upon Sc/Y and Sc/Ru substitution revealed Y and Ru preferring heptagonal- and hexagonal-prismatic environment, respectively. We also provide the information on phase relations and solubility ranges of compounds in the Sc-Ru-B system at 800 °C within 35-70 at.% B including binary boundaries. The crystal structures of the new compounds are discussed in relationship with known borides. Electronic structure calculations reveal the metallic character of $ScRu_2B_3$ and Sc_2RuB_6 in good agreement with electrical resistivity data.

EXPERIMENTAL SECTION

Synthesis and Phase Analysis. Alloys were prepared from ingots of pure elements (Ru pieces 99.9 mass %, crystalline boron 99.8 mass%, Sc pieces distilled 99.99 mass %, Y pieces 99.9 mass % - all obtained from ChemPur, Germany) by repeated arc melting under argon. The arc-melted buttons were cut into pieces, wherefrom one piece was wrapped in tantalum foil and vacuum-sealed in a quartz tube for annealing at 800 °C for 720 hours. The annealed samples were polished applying standard procedures and were examined by scanning electron microscopy (SEM) using a Philips XL30 ESEM with EDAX XL-30 EDX-detector to determine Sc/Ru ratios. Powder X-ray diffraction (XRD) data were collected employing a Guinier-Huber image plate system with monochromatic Cu $K_{\alpha 1}$ radiation ($8^\circ \leq 2\theta \leq 100^\circ$) from as-cast and annealed alloys. Quantitative Rietveld refinements of the powder XRD data were performed with the FULLPROF program[19] with the use of its internal tables for atom scattering factors.

Electrical Resistivity. The temperature dependent electrical resistivity of the compounds described above was studied using a four point probe technique and employing a Lakeshore 370 a.c. resistance bridge in the range from room temperature down to 4.2 K.

Computational Method. The calculations were performed within the DFT framework using the Quantum ESPRESSO package[20]. The correlation and exchange effects of the electrons were handled by using the generalized gradient approximation (GGA) of Perdew, Burke, and Ernzerhof, revised for solids (PBEsol)[21]. Electron-ion interactions were treated with the pseudopotential method[22,23] applying fully relativistic pseudopotentials constructed according to the code supplied by the PSLibrary (version 1.0.0)[24]. For scandium and ruthenium 3*s*- and 3*p*-, and 4*s*- and 4*p*- respectively were considered as valence states. The electron wave functions were expanded into plane waves with a kinetic energy cutoff of 816 eV. For the

charge density, a kinetic energy cutoff of 6530 eV was used. The k-point mesh for each compound had been constructed using Monkhorst–Pack method[25] on a grid of the size that guarantees less then 0.05×2π/Å spacing between the k-points for the calculations related to cell parameters optimization procedure and less then 0.03×2π/Å spacing for the final optimized cell relaxation. The convergence threshold for self-consistent-field iteration was set at 10^{-8} eV. The calculations were performed taking into account the spin-orbit interactions assuming the total magnetization to be zero.

To optimize the cell parameters for each compound, the total energies had been calculated for the cells with the cell parameters evenly distributed in all variable dimensions in the vicinity of the experimentally achieved data with the atomic positions being optimized according to BFGS algorithm. Further, the cell parameters corresponding to the minimal energy were obtained using interpolation, and for this cell parameters, the atomic positions were once again optimized until all forces became smaller than 10^{-5} eV/Å.

Crystal Structure Determination from Single Crystal XRD Data. All crystals were isolated via mechanical fragmentation of the annealed samples. Single crystal X-ray intensity data were collected on a four-circle Bruker APEX II diffractometer (CCD detector, κ-geometry, Mo Kα radiation). Multi-scan absorption correction was applied using the program SADABS; frame data were reduced to intensity values applying the SAINT-Plus package.[26] The structures were solved by direct methods and refined with the SHELXS-97 and SHELXL-97 programs,[27,28] respectively. Further details concerning the experiments are summarized in Table 1. Detailed descriptions of structural refinements are given below.

$ScRu_2B_3$. XRD data for the crystal, which was selected from the alloy $Sc_{17}Ru_{33}B_{50}$ annealed at 800 °C, were indexed with a *oC* unit cell with lattice parameters *a*=3.0195(2) Å, *b*=15.4056(8) Å and *c*=5.4492(3) Å. Systematic absences were consistent with three space groups, *Cmcm*, *Cmc*2_1 and *C*2*cm,* of which the centrosymmetric *Cmcm* proved to be correct during structure solution and refinement. Two Ru and one Sc atom positions were deduced from direct methods with SHELXS-97 and refined in a straightforward manner using SHELXL-97; two B sites were easily located in the difference Fourier map. The refinements with free site occupation factors showed full occupation of atom sites thus leading to a composition $ScRu_2B_3$ with four formula units per unit cell. As inferred from Rietveld refinement, powder XRD intensities collected from the polycrystalline alloys with nominal composition $Sc_{17}Ru_{33}B_{50}$ are in best agreement with the intensities calculated from the structural model taken from the single crystal. The final positional and atom displacement

parameters and interatomic distances obtained from single crystal are listed in Tables 1, 2, S1, S2.

Table 1. Structure Refinement Details from Single Crystal XRD[a]

Compound	$ScRu_2B_3$	Sc_2RuB_6	$Sc_{1.669}Y_{0.268}Ru_{1.063}B_6$
Nominal composition	$Sc_{16.67}Ru_{33.33}B_{50.00}$	$Sc_{22.22}Ru_{11.11}B_{66.67}$	$Sc_{18.54}Y_{2.98}Ru_{11.81}B_{66.67}$
Formula from refinement	$ScRu_2B_3$	Sc_2RuB_6	$Sc_{1.669}Y_{0.268}Ru_{1.063}B_6$
Theta range (deg)	$2.64<\theta<34.91$	$3.65<\theta<34.47$	$2.93<\theta<34.50$
Crystal size (μm)	55x65x50	54x43x28	50x42x31
Space group	*Cmcm* (No. 63)	*Pbam* (No. 55)	*Pbam* (No. 55)
Structure type	$ScRu_2B_3$	Y_2ReB_6	Y_2ReB_6
a (Å)	3.0195(2)	8.8545(2)	8.8846(4)
b (Å)	15.4056(8)	11.1620(3)	11.2073(5)
c (Å)	5.4492(3)	3.4760(1)	3.4904(2)
Z	4	4	4
Number of variables	25	58	62
Reliability factors[b]	R_F^2=0.0105;	R_F^2=0.0185;	R_F^2=0.0167;
-	R_{Int}=0.028	R_{Int}=0.035	R_{Int}=0.041
GOF	1.064	1.047	1.113
Extinction (Zachariasen)	0.0225(6)	0.0075(9)	0.0039(4)
Residual density; max;min ($e^-/Å^3$)	0.626; -1.008	0.955; -1.154	0.993; -0.910

[a]For all structures, T = 298(2) K, λ = 0.71073 Å and mosaicities of the crystals were <0.50.
[b]$R_F^2 = \Sigma|F_0^2-F_c^2|/\Sigma F_0^2$.

Sc_2RuB_6 and $Sc_{1.669}Y_{0.268}Ru_{1.063}B_6$. Unit cell dimensions of single crystals and X-ray powder diffraction spectra undoubtedly suggested isotypism with the Y_2ReB_6 structure[30], however single crystal studies have been undertaken in order to determine precisely the atom coordinates and evaluate the Sc, Ru and Y atom site preferences upon Sc/Y and Sc/Ru substitution. Direct methods applied to the single crystal XRD data delivered the structure solutions with three metal sites, which were consequently assigned to two Sc and one Ru for both crystals. Six boron atom positions were readily found in the difference Fourier map. Refinement of the occupancy of Sc and Ru positions for Sc_2RuB_6 crystal yielded no significant deviation from full positional occupation (largest Sc/Ru disorder <2.5% was detected for Sc2 leading to less than 10% improvement of reliability factor from R_F^2=0.0185 to R_F^2=0.0175), thus in the refinement of the final structure model full occupation was assumed (Tables 1, 2, S1). For the Sc/Y mixed crystal, the anomalously small atomic displacement parameter of the M1 site and residual electron density peak of 6.9 e/Å3 at 0.1 Å from M1 suggested a significant disorder for this atom site. Introducing a free variable for the mixed Sc/Y occupation of the 4*h* site resulted in 73.2(2)% Sc1 + 26.8(2)% Y1. Successive refinement cycles revealed a relatively large peak of electron density (5.9 $e^-/Å^3$) in the vicinity of Sc2 (at 0.42 Å); when refined freely, the occupancy of Sc2 resulted in 10% over-

occupancy implying the presence of a higher electron density. If this site was allowed to be occupied by a mixture of Sc and Y (i.e. 91%Sc+9%Y), the distances to the associated atoms are too short for Y, e.g. the shortest $d_{M2\text{-}B}$=2.477 Å, $d_{M2\text{-}Ru}$=2.7835 Å and $d_{M2\text{-}M2}$=2.962 Å in comparison with the shortest distances in $d_{Y2\text{-}B}$=2.582 Å, $d_{Y2\text{-}Ru}$=2.821 Å and $d_{Y2\text{-}Y2}$=3.180 Å in Y_2RuB_6[31]; moreover Sc2/Y2 disorder did not resolve completely the residual electron density problem. Thus, this site was allowed to be occupied by a mixture of Sc and Ru atoms. The refinement converged to 0.937(2)Sc2+0.063(2)Ru2 however spotted out the elongated Sc2/Ru2 thermal ellipsoid which could be resolved into two very closely separated split sites (<0.3 Å) reflecting the same occupancy ratio and rendering the final formula $Sc_{1.669}Y_{0.268}Ru_{1.063}B_6$. Final refinement offered the featureless electron density map ($\Delta\rho_{max}$=+0.99 $e^-/Å^3$, $\Delta\rho_{min}$=-0.91 $e^-/Å^3$) at R_F^2=0.0167 (Table 1, 2, S1). Bond lengths values of the two structures are listed in Table S3.

CIF data have been deposited with Fachinformationszentrum Karlsruhe, 76344 Eggenstein-Leopoldshafen, Germany [fax: (49) 7247-808-666; e-mail: crysdata@fiz-karlsruhe.de] with depository numbers CSD-433123 for $ScRu_2B_3$, CSD-433124 for Sc_2RuB_6, CSD-433125 for $Sc_{1.669}Y_{0.268}Ru_{1.063}B_6$ and CSD-433126 for RuB (described below).

RESULTS AND DISCUSSION

$ScRu_2B_3$: Structural Description and Analysis. The $ScRu_2B_3$ compound forms a new structure type of borides. The unit cell exhibits a packing of two slabs interleaving infinitively along the *b* axis (Figure 1a). Slab A is a puckered $B6^3$ monolayer (in a*c* plane) neighboring with metal (Sc/Ru) 3^6 nets (Figure 1e) while slab B represents a slightly distorted $CeCo_3B_2$-type[32] structure (Figure 1b). At variance with AlB2 structure (Figure 1c,f), the puckered boron hexagons in $ScRu_2B_3$ have a boat configuration, which is fairly unusual, however, exists, for example, in RuB_2[33,34] (Figure 1d,g) and YMo_3B_7[35,36]; in most AlB_2[37] related binary borides (*e.g.* ReB_2[38], Ru_2B_3[39], Mo_2B_4 and W_2B_4[40]) the corrugated six-membered rings are chair-like. The (Sc/Ru) 3^6 sheets are undulated as well, resembling the Ru nets in RuB_2[33,34]; accordingly, Sc1 is slightly displaced from the center of the hexagon in the adjacent $CeCo_3B_2$-type segment (slab B). The coordination polyhedron (CP) of Sc includes 20 atoms and by shape constitutes a half of face-capped hexagonal prism combined with a corrugated B1 hexagon capped with Ru (Figure 1h) Again like in $CeCo_3B_2$[32] (Figure 1i), the rectangular faces of the hexagonal prism's segment are capped with boron atoms (B2); one Sc is located against each hexagonal face at 3.0195(2) Å from the central Sc atom. The flat

hexagons in $[ScB_9Ru_9Sc_2]$ are formed by four Ru (2 Ru1 and 2 Ru2) and two B1 in contrast to six Co in $[CeB_6Co_{12}Ce_2]$ of $CeCo_3B_2$; substitution of Ru by B leads to severe distortion of the hexagonal prism hosting Sc. CP's around Ru atoms exhibit 17 and 14 vertices for Ru1 and Ru2 respectively; the latter corresponds to $[CoB_4Co_6Ce_4]$ in $CeCo_3B_2$ (Table S2, Figure S1). Alike the Sc polyhedron, the coordination environment of Ru1 includes a puckered boron six-membered ring, however, capped with Sc: $[Ru1B_8Ru_4Sc_5]$.

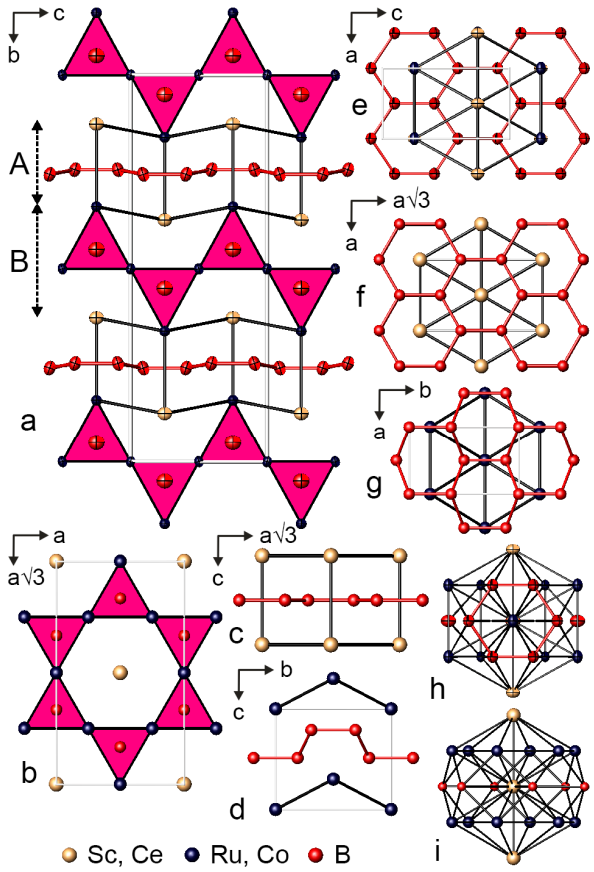

Figure 1. $ScRu_2B_3$ structure (a) in comparison with $CeCo_3B_2$ (b), ScB_2 (AlB_2-type) (c) and RuB_2 (d). Metal trigonal prisms around B in $ScRu_2B_3$ and $CeCo_3B_2$ are indicated; B-B bonds are shown as red sticks (light grey - in black-and-white version). Boron 6^3 nets and neighboring metal 3^6 nets in $ScRu_2B_3$ (slab A) (e), ScB_2 (f) and RuB_2 (g). CP's of Sc1 (h) and Ce (i) in $ScRu_2B_3$ and $CeCo_3B_2$, respectively.

B1-B1 interactions within $B6^3$ sheets are quite strong according to bond lengths: the distances $d_{B1\text{-}B1}$=1.713 Å and 1.827 Å are short in comparison with, for example, $d_{B\text{-}B}$=1.740 Å[34] (1.817 Å[41]) and 1.875 Å[34] (1.888 Å[41]) in RuB_2. CP of B1 in $ScRu_2B_3$ (distorted trigonal prism with three boron atoms located against rectangular faces, $[B1B_3Ru_3Sc_3]$) (Figure S1)

resembles the CP of B in AlB_2 rather than in RuB_2 ([$B1B_3Ru_3$], a trigonal pyramid completed by three borons located against the edges at the distance of 1.740 Å and 1.875 Å). The metal coordination around B2 ($CeCo_3B_2$-type block) is a trigonal prism formed by six Ru; three rectangular faces of the trigonal prism are capped by Sc (Figure S1).

Table 2. Atomic Coordinates[a] and Equivalent Isotropic Displacement Parameters[b,c]

	$ScRu_2B_3$	Sc_2RuB_6	$Sc_{1.669}Y_{0.268}Ru_{1.063}B_6$
M1	4*c* (0,*y*,¼) *y*=0.37370(3)	4*h* (*x*,*y*,½) *x*=0.31816(6), *y*=0.41415(4)	4*h* (*x*,*y*,½) *x*=0.31940(4), *y*=0.41414(3)
Occ.	1.00 Sc1	1.00 Sc1	0.732(2)Sc1+0.268(2)Y1
U_{eq}	0.00427(9)	0.00455(10)	0.00476(9)
M2	4*c* (0,*y*,¼) *y*=0.16085(1)	4*h* (*x*,*y*,½) *x*=0.44409(5), *y*=0.12630(4)	4*h* (*x*,*y*,½) *x*=0.4439(1), *y*=0.12714(8)
Occ.	1.00 Ru1	1.00 Sc2	0.937(2)Sc2
U_{eq}	0.00357(6)	0.00276(10)	0.0039(1)
M3	4*a* (0,0,0)	4*h* (*x*,*y*,½) *x*=0.13866(2), *y*=0.17978(2)	4*h* (*x*,*y*,½) *x*=0.13936(2), *y*=0.18036(1)
Occ.	1.00 Ru2	1.00 Ru3	1.00 Ru3
U_{eq}	0.00287(6)	0.00297(7)	0.00327(5)
M4	-	-	4*h* (*x*,*y*,½) *x*=0.455(1), *y*=0.1053(6)
Occ.	-	-	0.063(2)Ru2
U_{eq}	-	-	0.0039(1)
B	8*f* (0,*y*,*z*) *y*=0.2439(1), *z*=0.5928(3)	4*g* (*x*,*y*,0) *x*=0.0535(3), *y*=0.0649(3)	4*g* (*x*,*y*,0) *x*=0.0538(3), *y*=0.0658(2)
Occ.	1.0 B1	1.0 B1	1.0 B1
U_{eq}	0.0044(3)	0.0040(5)	0.0049(4)
B	4*c* (0,*y*,¼) *y*=0.5502(2)	4*g* (*x*,*y*,0) *x*=0.1024(3), *y*=0.4719(3)	4*g* (*x*,*y*,0) *x*=0.1013(3), *y*=0.4724(2)
Occ.	1.0 B2	1.0 B2	1.0 B2
U_{eq}	0.0055(4)	0.0040(5)	0.0052(4)
B	-	4*g* (*x*,*y*,0) *x*=0.1296(3), *y*=0.3176(2)	4*g* (*x*,*y*,0) *x*=0.1297(3), *y*=0.3174(2)
Occ.	-	1.0 B3	1.0 B3
U_{eq}	-	0.0047(5)	0.0050(4)
B	-	4*g* (*x*,*y*,0) *x*=0.2512(3), *y*=0.0784(2)	4*g* (*x*,*y*,0) *x*=0.2520(3), *y*=0.0796(2)
Occ.	-	1.0 B4	1.0 B4
U_{eq}	-	0.0047(5)	0.0049(4)
B	-	4*g* (*x*,*y*,0) *x*=0.2938(3), *y*=0.2359(2)	4*g* (*x*,*y*,0) *x*=0.2934(3), *y*=0.2358(2)
Occ.	-	1.0 B5	1.0 B5
U_{eq}	-	0.0046(5)	0.0050(4)
B	-	4*g* (*x*,*y*,0) *x*=0.4792(3), *y*=0.2875(2)	4*g* (*x*,*y*,0) *x*=0.4801(3), *y*=0.2868(2)
Occ.	-	1.0 B6	1.0 B6
U_{eq}	-	0.0041(5)	0.0050(4)

[a] Crystal structure data are standardized using the program Structure Tidy[29]. [b] U_{eq} is defined as one-third of the trace of the orthogonalized Uij tensor. [c] Anisotropic displacement parameters (U_{ij}) are given in Table S1

Binary AlB_2 related boride structures (RuB_2[33,34], ReB_2[38], Ru_2B_3[39], etc.) differentiate by modes of stacking of planar or puckered $B6^3$ layers and metal-atom layers[7]. Despite the occurrence of AlB_2-type related binary borides, no ternary representatives exhibiting infinite 2*D* hexagon-mesh B nets are known except for $Pr_5Co_2B_6$ where the $B6^3$ nets alternate with Pr_2Co- and Co- layers[42]. On the other hand, several boride structural series are based upon $CeCo_3B_2$-type intergrown with other structures,[43] e.g. $CaCu_5$, $MgZn_2$, $MgCu_2$, $ThCr_2Si_2$. A couple of metal- or boron-deficient representatives of the $CeCo_3B_2$-type have been known ($Ba_2Ni_9B_6$,[44] $NaPt_3B$,[45] $LaNi_3B$[46]) as well as the structure exhibiting $CeCo_3B_2$-type slabs

separated by hexagon-mesh metal nets in $PrRh_{4.8}B_2$[47]. $ScRu_2B_3$ is so far a unique example where the stacking of $CeCo_3B_2$-type fragments is realized via an intercalated AlB_2-type related structure exhibiting well developed boron 6^3-nets. More precisely the structure can be described in topochemical mode as

2 ("$ScRu_3B_2$") ($CeCo_3B_2$-type)+2 ("$ScRuB_4$") (hypothetical AlB_2-type derivative)=4 $ScRu_2B_3$.

Y_2ReB_6-type compounds. Both Sc_2RuB_6 and $Sc_{1.669}Y_{0.268}Ru_{1.063}B_6$ adopt the Y_2ReB_6 type[30] structure. Similar to $ScRu_2B_3$, these compounds also assume the 2D boron net formation (Figure 2). However, here the boron nets are planar and consist of irregular pentagonal, hexagonal and heptagonal B rings; metal atoms are found in prismatically coordinated centers in the interlayer spaces between the neighbouring boron sheets. Ru occupies the center of a pentagonal prism both in purely Sc and Sc/Y disordered structures (Figure 2, S2); excess of Ru tends to replace partially Sc inside the hexagonal void formed by boron atoms (Figure S2). Coordination spheres for the atoms in the $Sc_{1.669}Y_{0.268}Ru_{1.063}B_6$ structure when the split site Sc2/Ru2 is considered replicate the shape of those in Sc_2RuB_6 differentiating slightly in coordinating distances due to small shifts of atom positions (Table S3). The center of the larger heptagonal prismatic void (shortest $d_{M1\text{-}B4}$ is 2.624(1) Å as compared to $d_{Sc2\text{-}B2}$ of 2.481(2) Å) is prone to sizable Sc/Y substitution. Each boron atom is coordinated by six metal atoms in a trigonal prismatic manner, with all three rectangular faces capped with boron atoms (Figure S2). The B—B bond lengths (Table S3) are very close to the bonds found in Sc_2RhB_6[12]. Notably the long contact distance between two B2 atoms shared by hexagonal rings and inter-linking the heptagonal rings (1.919(4) Å and 1.903(4) Å for Sc_2RuB_6 and $Sc_{1.669}Y_{0.268}Ru_{1.063}B_6$, respectively) appears to be a common feature of Y_2ReB_6-type compounds[48] (e.g. 2.134 Å in Y_2ReB_6,[30] 2.148 Å in Gd_2RuB_6,[31] 1.929 Å in Sc_2RhB_6[12]). The remaining B—B bond lengths vary between 1.716(4) Å - 1.798(5) Å and 1.719(4) Å - 1.789(3) Å for Sc_2RuB_6 and $Sc_{1.669}Y_{0.268}Ru_{1.063}B_6$, respectively.

$ScRu_2B_3$ and Sc_2RuB_6: Ternary Phase Diagram in the Relevant Concentration Area. Our reinvestigation of the binary Sc-B and Ru-B systems pertinent to the concentration areas of the current study at 800 ºC by powder XRD confirmed the existence and crystal structure of ScB_2, RuB_2 and Ru_2B_3 in essential consistency with literature data[49-52]. However, earlier studies on the Ru-B phase diagram from powder XRD data left open the question about composition and structure type of $RuB_{\sim 1.1}$. According to Arronsson et al.[53], the hexagonal compound (identical to the one reported by Kempter and Fries (AlB_2-type)[54]), forms in the Ru-B system with high deviation from the "ideal" composition. In order to clarify whether the boron atoms are distributed statistically in boron deficient AlB_2-type or in an

ordered way over the possible positions in WC-type we have performed the investigation of this phase applying single crystal XRD. A structure analysis has been attempted on a single crystal specimen mechanically isolated from the sample annealed at 800 ºC with nominal composition $Ru_{50}B_{50}$ (in at.%). Single crystal XRD data were completely indexed in a hexagonal lattice; the analysis of the systematic extinctions suggested among others ($P\bar{6}2m$, $P\bar{6}m2$, *P*622, *P6mm*, $P\bar{6}$, *P*6, *P*6/*m*) the space group *P*6/*mmm* as the one with the highest symmetry. Structure solution prompted ruthenium atom in 1*a* (0,0,0) and revealed a peak of electron density in 2*d* (⅓,⅔,½) which could correspond to B atoms. Subsequent refinements rendered about 50% occupancy for the boron site. Further ordering of boron vacancies was achieved in the $P\bar{6}m2$ (no. 187) space group (B in 1*d* (⅓,⅔,½); Occ. 1.0; WC- type structure, Table S4); refinement of occupancies have not indicated any vacancies in the Ru subnet (Ru in 1*a* (0,0,0)) defining the RuB-phase composition at 50.0 at.% B.

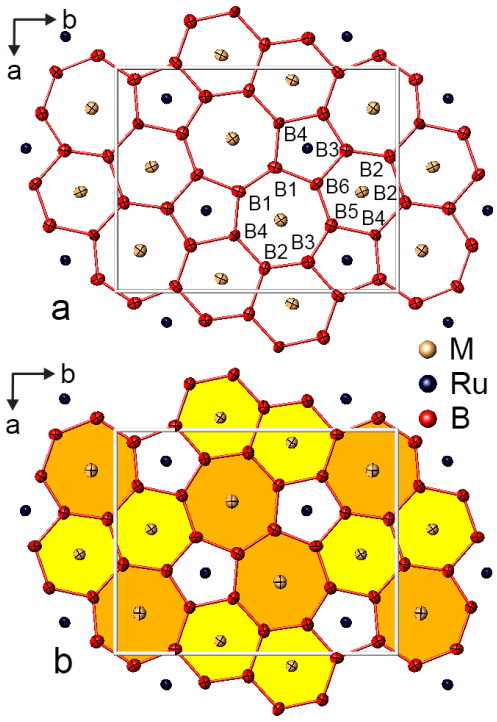

Figure 2. Projection of Sc_2RuB_6 (a) and $Sc_{1.669}Y_{0.268}Ru_{1.063}B_6$ (b) structures along the *c*-axis highlighting the hexagonal and heptagonal channels hosting Sc1/Y1 (light brown; dark grey in black-and-white version) and Sc2/Ru2 (yellow; light grey in black-and-white version) mixtures respectively. Ru2 in split position is omitted for clarity. M stands for Sc, Sc/Y and Sc/Ru.

Rietveld refinement of powder XRD data of the alloys annealed at 800 ºC showed a full occupancy of the Ru atom site for the B-poor region (*a*=2.85032(3) Å, *c*=2.85564(4) Å, *V*=20.092 Å^3), from the $Ru_{55}B_{45}$ two-phase alloy with $Ru_{11}B_8$ as a secondary phase. For the refinement of powder XRD data collected from the B-rich sample, the AlB_2 structure model was employed leading to $Ru_{46.5}B_{53.5}$ (at.%) composition formula at 57.5% B occupancy of Wyckoff site 2*d* (*a*=2.85267(3) Å, *c*=2.85497(4) Å, *V*=20.120 Å^3; $Ru_{45}B_{55}$ two-phase alloy containing Ru_2B_3 as a secondary phase). According to EPMS and powder XRD data of ternary samples annealed at 800 ºC, the $RuB_{1-1.15}$ binary dissolves less than 4 at.% Sc; no solubilities of Sc were found for RuB_2 and Ru_2B_3. A deviation of scandium diboride from stoichiometric composition ($Sc_{1-x}B_2$, x=0.06, AlB_2-type) has been found from the boron rich ternary samples annealed at 800 ºC; the solubility of Ru in $Sc_{1-x}B_2$ is rather small (about 3 at.% Ru) in comparison with related Sc-T-B (T=W, Re, Cr)[55,56] diborides.

Previous knowledge on the ternary Sc-Ru-B phases was limited to the investigation of as cast alloys from late 1970[thies 9] amended by the data on the crystal structure of $Sc_2Ru_5B_4$[10]. In the current work we confirmed the existence and structural features of $Sc_2Ru_5B_4$ and identify two new compounds, $ScRu_2B_3$ and Sc_2RuB_6 from the alloys annealed at 800 ºC (Figure 3). In contrast to related systems with compatible r_T/r_M ratios ($Lu_{1.34}V_{1.66}B_6$,[57] (ZrCr)CrB_6[58]), powder XPD and EPMA data yielded a relatively small Sc/Ru exchange at constant boron content in Sc_2RuB_6 (up to 91% Sc2 + 9% Ru2 in 4*h*; Rietveld refinement of powder XRD data). No significant homogeneity range has been observed for $ScRu_2B_3$. There is no indication for the presence of a phase ‘‘$ScRuB_4$’’ as reported by Ku et al.[9]: XRD patterns of both as cast and quenched at 800 ºC alloys at this composition yield the two-phase region $Sc_{2-x}Ru_{1+x}B_6$+RuB_2. The phase relations derived at 800°C are also consistent with the nonexistence of "$ScRuB_2$" (see ref.[59]) as well as validate the identity of $ScRu_{\sim 2}B_{\sim 2}$, claimed by Ku et al.[9] with $Sc_2Ru_5B_4$[10]. Variations of lattice parameters in ternary alloys near the $Sc_{2+x}Ru_{5-x}B_4$ composition (*a*=8.5054(1) Å - 8.5679(2) Å, *b*=2.99199(4) Å - 3.01431(7) Å, *c*=9.9809(1) Å - 9.9762(3) Å, *β*=90.029(3)º - 90.132(2)º for Sc-poor and Sc-rich samples, respectively) indicate the existence of a ternary homogeneity region; the solid solution extends to a limit at x=0.6 as inferred from the EPMA ratio Sc/Ru=34.2/65.8. The well known superconducting $ScRu_4B_4$[9] phase does not exist at 800 ºC, however, it is present in the powder XRD patterns of alloys in as cast condition along with $ScRu_2B_3$, $Sc_{2+x}Ru_{5-x}B_4$ and ruthenium monoboride. Consistent with literature data, lattice parameters were obtained from powder XRD data for $ScRu_4B_4$ (*a*=7.3543(2) Å, *c*=14.92137(8) Å) being in good agreement with lattice constants calculated from ab initio techniques (see below).

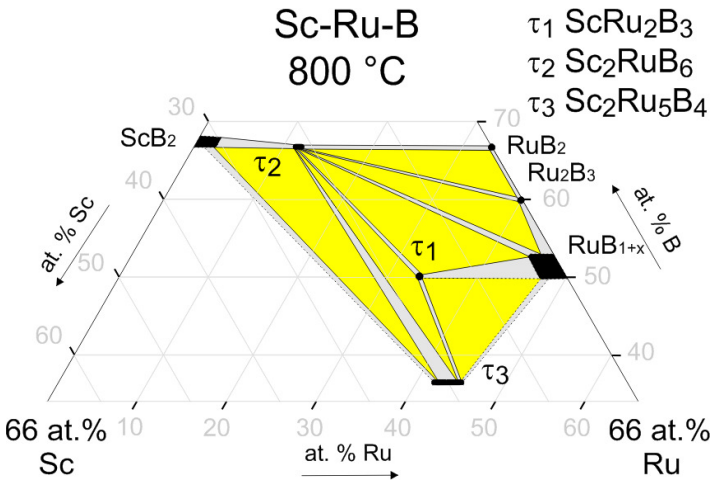

Figure 3. Partial isothermal section of the Sc-Ru-B system at 800 °C within ca. 35 - 70 at.% B. White areas and dashed lines indicate unexplored regions and tentative equilibria, respectively.

Cell Optimization and Density of States (DOS). To prove the correctness of both, the crystallographic models and the chosen pseudopotentials, we firstly optimize the lattice constants of $ScRu_2B_3$, Sc_2RuB_6 and $ScRu_4B_4$ to obtain the relaxed structures. The initial lattice parameters are taken from experimental data as a starting point for geometry optimization. The calculated lattice parameters are listed in Table 3 in comparison with experimental values; additionally, the calculated zero-temperature energy of $ScRu_4B_4$ as a function of lattice constants is shown in Figure 4. It is seen that in general the lattice constants obtained as results of DFT calculation are in very good agreement with the experimental data indicating the properness of the initial assumptions. The highest deviation between the observed and calculated data (~1%) has been found for the *b* parameter of $ScRu_2B_3$. Moreover, the refined atomic coordinates for all compounds are almost identical to the values deduced from X-ray diffraction.

Table 3. Optimized vs Experimental Lattice Constants

	a (Å)	*b* (Å)	*c* (Å)
	$ScRu_2B_3$ (space group *Cmcm*)		
Calculated	3.0189	15.2602	5.4425
Experimental (single crystal XRD)	3.0195(2)	15.4056(8)	5.4492(3)
	Sc_2RuB_6 (space group *Pbam*)		
Calculated	8.8253	11.1549	3.4409
Experimental (single crystal XRD)	8.8545(2)	11.1620(3)	3.4760(1)
	$ScRu_4B_4$ (space group $I4_1/acd$)		
Calculated	7.3239	-	14.8726
Experimental (powder XRD)	7.3543(2)	-	14.92137(8)

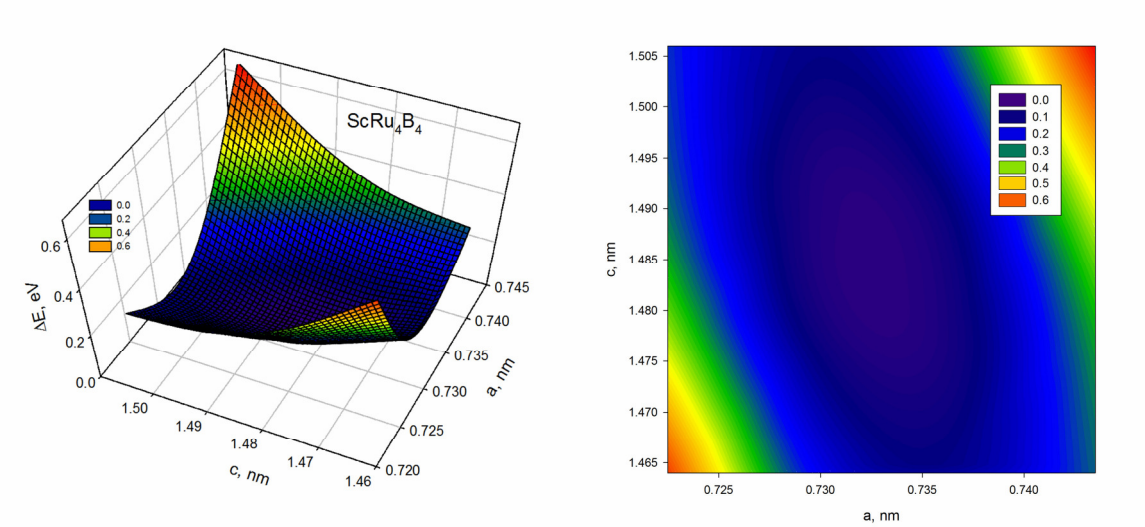

Figure 4. Relative energy of formation of $ScRu_4B_4$ unit cell depending on the cell parameters in 3D and projected to plane. 0 eV are associated with the stable configuration.

Table 4. Calculated Atomic Coordinates

$ScRu_2B_3$	Sc_2RuB_6
Sc1 in 4*c* (0,*y*,¼) *y*=0.372699348	Sc1 in 4*h* (*x*,*y*,½) *x*=0.318185864, *y*=0.414011790
Ru1 in 4*c* (0,*y*,¼) *y*=0.161982819	Sc2 in 4*h* (*x*,*y*,½) *x*=0.443701492, *y*=0.127175771
Ru2 4*a* (0,0,0)	Ru3 in 4*h* (*x*,*y*,½) *x*=0.138608848, *y*=0.179750930
B1 in 8*f* (0,*y*,*z*) *y*=0.244040520, *z*=0.592006111	B1 in 4*g* (*x*,*y*,0) *x*=0.053571135, *y*=0.064832400
B2 in 4*c* (0,*y*,¼) *y*=0.550328169	B2 in 4*g* (*x*,*y*,0) *x*=0.101427764, *y*=0.472236508
-	B3 in 4*g* (*x*,*y*,0) *x*=0.129545668, *y*=0.317752268
-	B4 in 4*g* (*x*,*y*,0) *x*=0.251860023, *y*=0.078491613
-	B5 in 4*g* (*x*,*y*,0) *x*=0.293566521, *y*=0.235882221
-	B6 in 4*g* (*x*,*y*,0) *x*=0.479352435, *y*=0.287408313

The total density of states in the vicinity of the Fermi energy for the studied compounds is presented in Figure 5 along with partial DOS's for various atoms. All compounds demonstrate a nonvanishing density of states at the Fermi energy, hinting towards metallic behavior of these systems.

The Fermi level of $ScRu_2B_3$ is located on the right shoulder of a pseudogap in the DOS (Figure 5) with a calculated density of states $N(E_F)$=2.84 eV^{-1} $f.u.^{-1}$. The Ru(*d*) states dominate between -5 and 0 eV (E_F). They start to decrease below -6 eV, demonstrating a gap-like behavior near -7 eV and than contribute to a peak at -9 eV. The Sc(*d*) contributions appear at about -1.9 eV and -3.5 eV while the contribution of *s*-states of Sc is almost negligible. *S*- and *p*-states of B1 dominate the DOS in the region between -10 and -13 eV with *p*-states extending up to -3 eV. *S*-states of B2 participate in formation of a peak around -9 eV, almost not overlapping with the B2 *p*-states, which are pronounced at around -5 eV. Strictly on the Fermi level the DOS is determined by Ru1(*d*) states with value of 1.5 eV^{-1} $f.u.^{-1}$. The average orbital energy of each boron species was calculated as the center of gravity of the

corresponding partial DOS. It is equal to -6.26 eV for B2 while the energy of B1 is for 0.4 eV lower indicating the presence of strong B1-B1 covalent bonding in agreement with structural data.

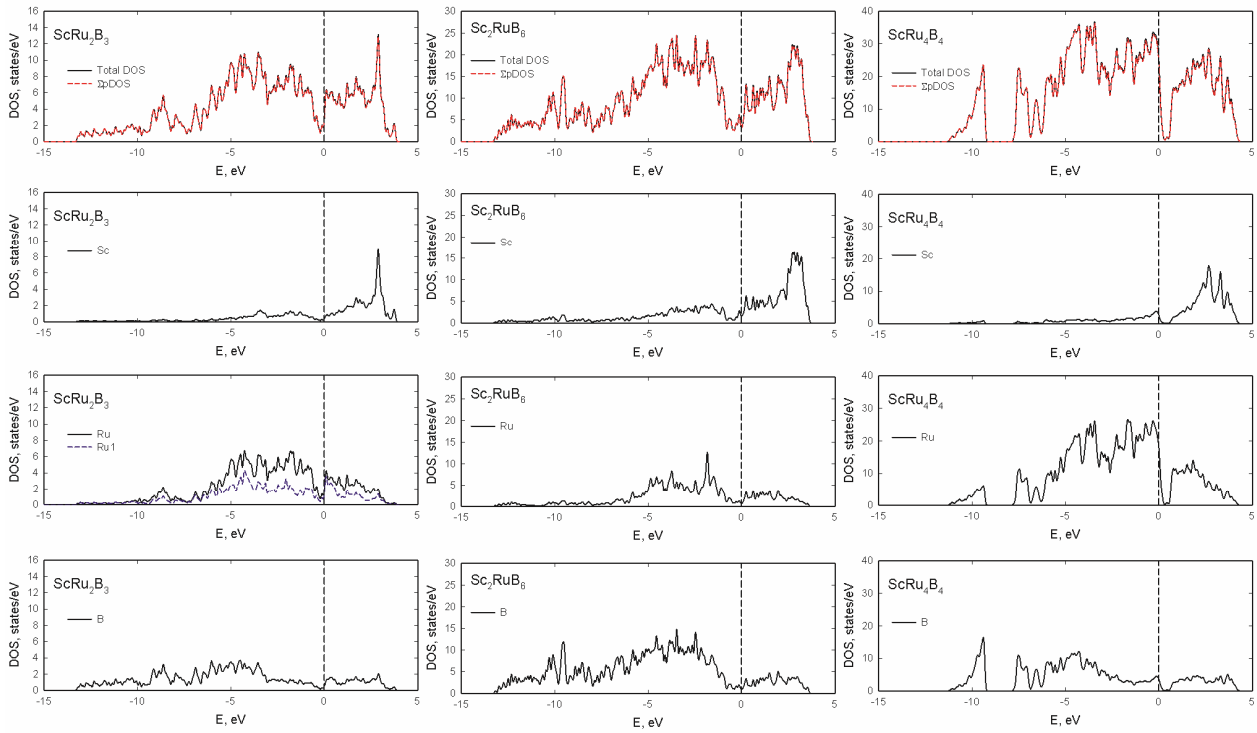

Figure 5. Total electronic density of states, the sum of partial DOS's and the partial contribution for different atoms for $ScRu_2B_3$, Sc_2RuB_6 and $ScRu_4B_4$. Graphs are constructed taking into account the multiplicity of the equiatomic positions. On these graphs the plots for the individual electron states for atoms are omitted to preserve the overall readability.

The pseudo-gap in the DOS (Figure 5) of Sc_2RuB_6 is less pronounced and the calculated density of states on the Fermi level is about 3.15 eV^{-1} $f.u.^{-1}$. Sc, Ru and B more or less equally contribute to this value, although in the region below 0 eV the density of states is dominated by the B *p*-states along with the *d*-states of Sc. The relative contribution of Sc to the overall DOS decrease further simultaneously with the impact of Ru until, at around -6 eV, the density of states is almost totally formed by the relative B(*p*) states. The peak around -9 eV is produced equally by *s*- and *p*-states of boron atoms. The values obtained for the average orbital energy of B1, B4, B5 and B6 are close to -6.05 eV while they are significantly lower for B2 and B3 (-5.872 eV and -5.31 eV respectively). For the former one such a difference is originated by the qualitatively different surroundings of the atom, where B2, unlike the other borons, is not interacting with ruthenium. B3 on the other hand has a crystallographic

configuration similar to, *e.g.*, B1. The careful evaluation of *p*-states density (Figure 6) in comparison with the DOS of B1, however, reveals a much weaker B3-Sc1 bonding.

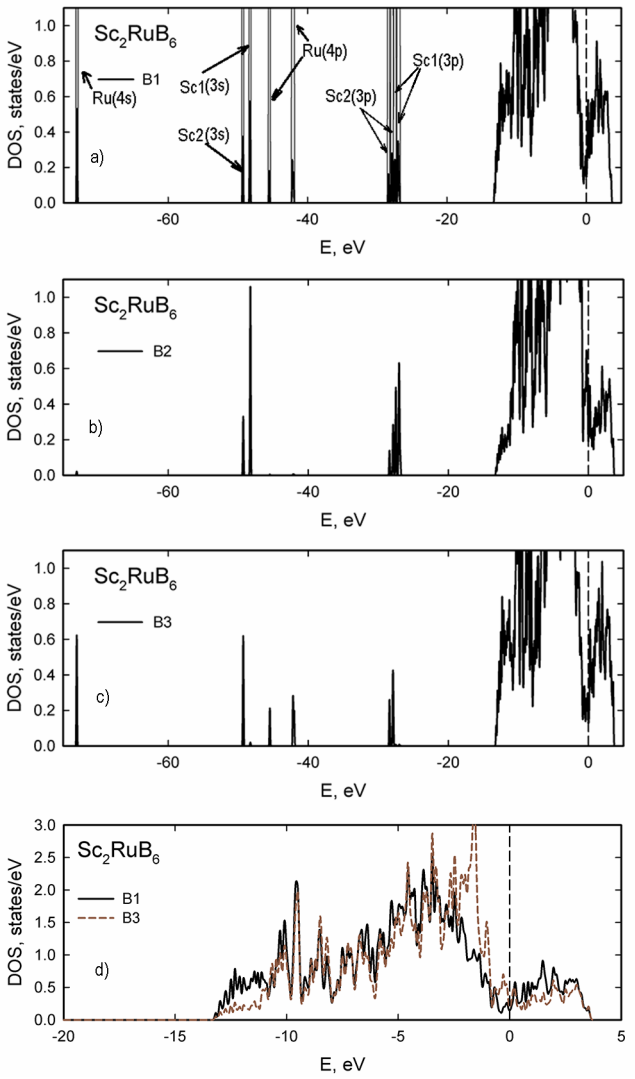

Figure 6. Density of states of boron atoms situated at the different atomic positions in Sc_2RuB_6 (a - B1, b - B2, c - B3) in the whole energy region studied. Marks on the B1 graph correspond to electron states, that dominate DOS at corresponding energies. d) DOS of B1 and B3 of Sc_2RuB_6 in the vicinity of the Fermi level.

The density of states of $ScRu_4B_4$ in the vicinity of the Fermi level (Figure 5) is entirely dominated by the Ru 4*d*-states, until the B *p*-states start to have a reasonable weight in the total DOS close to -4 eV. Near -6 eV the partial density of states of Ru strongly overlaps with that of B while the density of states of Sc bears an almost negligible value. With the decrease of energy, the total density of states of $ScRu_4B_4$ develops a gap between -7.8 and -9.2 eV, followed by a B (*p*) dominated peak near -9.5 eV. Although, at the Fermi level the density of

states is reasonably high (~ 24 eV^{-1} $f.u.^{-1}$), it is followed by the pronounced pseudo-gap in the conduction band around 0.4 eV as a result of strong chemical interaction. Ru-B covalent bonding is believed to be responsible for this effect[60]. The large transition-metal DOS from the Ru contribution indicates that a crucial requirement for the occurrence of superconductivity is satisfied[61].

Electrical Resistivity. Electrical resistivity of $ScRu_2B_3$, Sc_2RuB_6, RuB and RuB_2 has been studied using a 4-point method in a region from room temperature down to 4.2 K (Fig. 7). RuB and RuB_2 demonstrate a metal like behavior without any transitions in the entire temperature range. The electrical resistivity of these binaries is well described by

$$\rho(T) = \rho_0 + C\frac{T^5}{\theta_D{}^6}\int_0^{\theta_D/T}\frac{x^5}{(e^x-1)(1-e^{-x})}dx \qquad \text{(Eqn. 1)}$$

where ρ_0 is the residual resistivity. The second term in Eqn. 1 accounts for the temperature dependent electron-phonon scattering (Bloch-Grüneisen formula); C describes the electron-phonon coupling strength and θ_D is the Debye temperature.

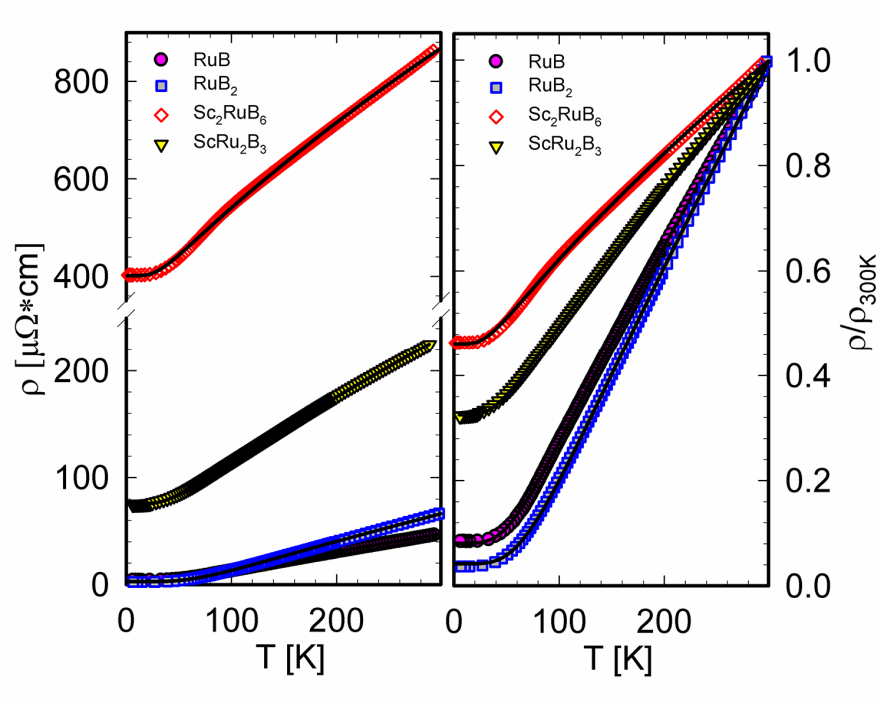

Figure 7. Temperature dependent electrical resistivity of compounds and the same data represented as ρ / ρ_{300K}. Solid lines correspond to models described in text.

In accordance with the finite values of the density of states at the Fermi energy, the resistivity of both $ScRu_2B_3$ and Sc_2RuB_6 behave metallic in the entire temperature interval. The Fermi energy is located in a region where the density of states has a tendency to increase, implying that electrons are the primary charge carriers in these ternary materials. The resistivity *vs* T dependencies of both compounds, however, demonstrate a significant curvature at around 50-100 K (more pronounced for Sc_2RuB_6) and is much better described adding an AT^3 term (Mott-Jones term) to Eqn. 1. The latter is included to account for *s-d* interband scattering at the Fermi level[62,63]. Sc_2RuB_6 is also characterized by a low RRR ($RRR = \rho_{300} / \rho_0$) value of ~2, indicating rather high degree of disorder in the sample and by a high overall resistivity, presumably due to the somewhat higher density of *d*-states at the Fermi level.

Values of residual resistivity ρ_0, Debye temperature θ_D, residual resistivity ratio values RRR and, where applicable, values of Mott coefficient A obtained as the result of a fit of the described models to the experimental data are summarized in Table 5.

Table 5. Residual Resistivity Ratio and List of Least Squares Fit Parameters, Derived for the Compound Using the Fit Models Described in Text

	ρ_0 ($\mu\Omega cm$)	θ_D (K)	A ($\mu\Omega cm / K^3$)	*RRR*
RuB	2.8	408	-	12.3574
RuB_2	3.9	324	-	23.9131
Sc_2RuB_6	401	183	$9.4x10^{-7}$	2.1657

CONCLUSIONS

The Sc-Ru-B system has been studied with respect to formation and crystal structure of compounds exhibiting extensive B bonding. Two novel ternary borides, $ScRu_2B_3$ and Sc_2RuB_6 were identified and their atomic arrangements were determined from single crystal X-ray diffraction data. $ScRu_2B_3$ crystallizes in its own structure type while Sc_2RuB_6 is a new member of the Y_2ReB_6-type family. $ScRu_2B_3$ exhibits an unusual architecture combining the $CeCo_3B_2$- and AlB_2-type related slabs interleaving infinitely along the *b* axis which can be described in topochemical mode as 2 ("$ScRu_3B_2$") ($CeCo_3B_2$-type)+2 ("$ScRuB_4$") (hypothetical AlB_2-type derivative)=4 $ScRu_2B_3$. In Sc_2RuB_6 and isotypic $Sc_{1.669}Y_{0.268}Ru_{1.063}B_6$ the peculiar boron 6^3 nets of AlB_2-type are modified to form planar boron pentagons, hexagons and heptagons. Distribution of atoms on three metal sites follows the tendency observed for rare earth transition metal borides; excess of Ru replaces Sc inside the boron hexagonal prismatic void. Boron atoms in both structures are in trigonal prismatic

coordination. Whilst size and shape of boron aggregation in Sc_2RuB_6 correlate well with the atomic percentage of boron and metal (66.6 at.% B; M/B=0.5) exhibiting 2*D* planar nets of condensed boron polygons, the boron aggregation in $ScRu_2B_3$ (M/B=1) is different from what is expected according to the classification scheme of borides[7]. Phase relations in the Sc-Ru-B system at 800 ºC within the concentration range studied are governed by three ternary compounds, $ScRu_2B_3$, Sc_2RuB_6 and $Sc_2Ru_5B_4$; Ru/Sc substitution in the later compound attains *ca*. 3.5 at.%. Solubilities of Sc in binary ruthenium borides in the relevant concentration range are negligible except for $RuB_{1-1.15}$ which dissolves up to *ca*. 4 at.% Sc. In RuB, boron atoms are distributed in an ordered way over the possible positions of the WC-type. Extension of ScB_2 in the ternary system is limited to 3 at.% Ru at 800 ºC. The lattice parameters and atomic coordinates were calculated for $ScRu_2B_3$, Sc_2RuB_6 and $ScRu_4B_4$ with high accuracy within the DFT framework showing a good agreement with the experimentally obtained values. The density of states in Sc_2RuB_6 at the Fermi level is more or less equally originated by the outer Sc, Ru and B states, while in $ScRu_4B_4$ it is almost completely produced by 4*d*-states of Ru atoms, and the 4*d*-states of Sc are strongly overlapped with the B 2*p*-states in the vicinity of 0 eV. In $ScRu_2B_3$, on the other hand, only the Ru1 *d*-shell plays a significant role in the formation of the states around the Fermi level. Resistivity studies revealed a metallic behavior in all cases, in agreement with the finite value of the electronic density of states at the Fermi energy.

ACKNOWLEDGEMENTS

The research work of O.S. was supported by Austrian FWF project V279-N19.

ASSOTIATED CONTENT

Supporting Information

Anisotropic displacement parameters data and interatomic distances for $ScRu_2B_3$, Sc_2RuB_6 and $Sc_{1.669}Y_{0.268}Ru_{1.063}B_6$; Coordination polyhedra of atoms; X-ray crystallographic file for $ScRu_2B_3$, Sc_2RuB_6, $Sc_{1.669}Y_{0.268}Ru_{1.063}B_6$ and RuB in CIF format.

The Supporting Information is available free of charge on the ACS Publications website at DOI:.....

AUTHOR INFORMATION

Corresponding Author

**E-mail address: oksana.sologub@univie.ac.at*

Notes

The authors declare no competing financial interest.

REFERENCES

(1) Johnston, D.C. Superconductivity in a new ternary structure class of boride compounds. *Solid State Comm.* **1977**, *24*, 699-702.

(2) Wolowiec, C.T.; White, B.D.; Maple, M.B. Conventional magnetic superconductors. *Physica C* **2015**, *514*, 113–129.

(3) Matthias, B.T.; Corenzwit, E.; Vandenberg, J.M.; Barz, H.E. High superconducting transition temperatures of new rare earth ternary borides. *Proc. Natl. Acad. Sci. USA* **1977**, *74(4)*, 1334-1335.

(4) Vandenberg, J.M.; Matthias, B.T. Crystallography of new ternary borides. *Proc. Natl. Acad. Sci. USA,* **1977**, *74(4)*, 1336-1337.

(5) Grottner, A.; Yvon, K. Lanthanum ruthenium boride, $LaRu_4B_4$. *Acta Crystallogr.* **1979**, *B35*, 451-453.

(6) Yvon, K.; Johnston, D.C. Orthorhombic $LuRh_4B_4$ - a new polytype of RT_4B_4 stoichiometry. *Acta Crystallogr. B* **1982**, *38*, 247-250.

(7) Rogl P., Existence and Crystal Chemistry of Borides, in *Inorganic Reactions and Methods;* Zuckerman, J.J., Ed.; VCH-Publications Inc. **1991**, 13(6), 85 and references therein.

(8) Ku, H.C.; Shelton, R.N. Superconductivity of new ternary borides with the $LuRuB_2$-type structure. *Mat. Res. Bull.* **1980**, *15*, 1441-1444.

(9) Ku, H.C.; Johnston, D. C.; Matthias, B.T.; Barz, H.; Burri, G.; Rinderer, L. $ScRu_4B_4$: A new superconducting member of the MRu_4B_4 ternary system. *Mater. Res. Bull.* **1979**, *14*, 1591.

(10) Rogl, P. The crystal structure of $Sc_2Ru_5B_4$. *J. Solid State Chem.* **1984**, *55*, 262-269.

(11) Zavalii, L.V.; Kuz'ma, Yu.B.; Mikhalenko, S.I. New scandium borides with a structure of the $YCrB_4$ type. *Inorg. Mater.* **1988**, *24*, 1549-1551.

(12) Salamakha, P.S.; Rizzoli, C.; Salamakha, L.S.; Sologub, O.L.; Goncalves, A.; Almeida, M. On the crystal structure of Sc_2MB_6 (M= Rh, Ir) compounds. *J. Alloys Compd.* **2005**, *396*, 240-242.

(13) Schiffer, J.; Jung, W. $MgOs_3B_4$ and $ScOs_3B_4$, ternary borides with a new channel structure. *J. Solid State Chem.* **2000**, *154*, 232-237.

(14) Shelton, R.N.; Karcher, B.A.; Powell, D.R.; Jacobson, R.A.; Ku, H.C. Crystal structure of $LuRuB_2$. *Mater. Res. Bull.* **1980**, *15*, 1445-1452.

(15) Rogl, P.; Nowotny, H. Studies of the (Sc,Zr,Hf)-(Rh,Ir)-B systems. *J. Less-Common Met.* **1979**, *67*, 41-50.

(16) Salamakha, L.; O. Sologub, O.; Rizzoli, C.; Michor, H.; Gonçalves, A.P.; Rogl, P.; Bauer, E. Crystal structure and physical properties of UMo_3B_7. *Intermetallics*, **2017**, *85*, 180-186.

(17) Sologub, O.; Salamakha, L.; Stöger, B.; Michiue, Yu.; Mori, T. Zr doped b-rhombohedral boron: widely variable Seebeck coefficient and structural properties. *Acta Mat*. **2017**, *122*, 378-385.

(18) Sologub, O.; Salamakha, L.P.; Stöger, B.; Rogl, P.F.; Michor, H.; Bauer, E. Incorporation of platinum atoms in a silicon-free boride of the YB_{50}-type structure. *J. Alloys Comp*. **2016**, *675*, 99-103.

(19) Rodríguez-Carvajal, J. Recent developments of the program FULLPROF. In *Commission on Powder Diffraction (IUCr). Newsletter* **2001**, *26*, 12-19.

(20) Giannozzi, P.; Baroni, S.; Bonini, N.; Calandra, M.; Car, R.; Cavazzoni, C.; Ceresoli, D.; Chiarotti, G. L.; Cococcioni, M.; Dabo, I.; Dal Corso, A.; de Gironcoli, S.; Fabris, S.; Fratesi, G.; Gebauer, R.; Gerstmann, U.; Gougoussis, C.; Kokalj, A.; Lazzeri, M.; Martin-Samos, L.; Marzari, N.; Mauri, F.; Mazzarello, R.; Paolini, S.; Pasquarello, A.; Paulatto, L.; Sbraccia, C.; Scandolo, S.; Sclauzero, G.; Seitsonen, A. P.; Smogunov, A.; Umari, P.; Wentzcovitch, R. M. QUANTUM ESPRESSO: a modular and open-source software project for quantum simulations of materials. *J. Phys.: Condens. Matter* **2009**, *21*, 395502.

(21) Perdew, J.P.; Ruzsinszky, A.; Csonka, G.I.; Vydrov, O.A.; Scuseria, G.E.; Constantin, L.A.; Zhou, X.; Burke, K. Restoring the density-gradient expansion for exchange in solids and surfaces. *Phys. Rev. Lett.* **2008**, 100, 136406; Erratum *Phys. Rev. Lett.* **2009**, *102*, 039902.

(22) Vanderbilt, D. Soft self-consistent pseudopotentials in a generalized eigenvalue formalism. *Phys. Rev. B: Condens. Matter Mater. Phys.* **1990**, *41*, 7892–7895.

(23) Laasonen, K.; Pasquarello, A.; Car, R.; Lee, C.; Vanderbilt, D. Car-Parrinello molecular dynamics with Vanderbilt ultrasoft pseudopotentials. *Phys. Rev. B* **1993**, *47*, 10142.

(24) Dal Corso, A. Pseudopotentials periodic table: from H to Pu. *Comput. Mater. Sci.* **2014**, *95*, 337–350.

(25) Monkhorst, H. J.; Pack, J. D. Special points for Brillouin-zone integrations. *Phys. Rev. B* **1976**, *13*, 5188–5192.

(26) Bruker. APEXII, RLATT, SAINT, SADABS and TWINABS. Bruker AXS Inc., Madison, Wisconsin, USA, **2014**.

(27) Sheldrick, G.M. SHELXS-97, Program for the solution of crystal structures, University of Göttingen: Germany, **1997**.

(28) Sheldrick, G.M. SHELXL-97, Program for crystal structure refinement, University of Göttingen: Germany, **1997**.

(29) Parthé, E.; Gelato, L.; Chabot, B.; Penzo, M.; Censual, K.; Gladyshevskii, R. TYPIX – standardized data and crystal chemical characterization of inorganic structure types, Springer: Berlin, **1994**.

(30) Kuz'ma, Yu. B.; Svarichevskaya, S. Crystal structure of Y_2ReB_6 and its analogs. *Kristallografiya* **1972**, *17*, 658–661.

(31) Hiebl, K.; Rogl, P.; Nowotny, H. Magnetism and structural chemistry of ternary borides RE_2MB_6 (RE= rare earth, M= Ru, Os). *J. Solid State Chem.* **1984**, *54*, 414-420.

(32) Kuz'ma, Yu.B.; Krypyakevych, P.I.; Bilonizhko, N.S. Crystal structure of $CeCo_3B_2$ and analogous compounds. *Dopov. Akad. Nauk Ukr. RSR* Ser. A **1969**, 939-941.

(33) Aronsson, B. The crystal structure of RuB_2, OsB_2 and $IrB_{1.35}$ and some general comments on the crystal chemistry of borides in the composition range MeB-MeB_3. *Acta Chem. Scand.* **1963**, 17, 2036-2050.

(34) Roof, R.B.; Kempter, C.P. New orthorhombic phase in the Ru-B and Os-B systems. *J. Chem. Phys.* **1962**, *37*, 1473-1476.

(35) Mikhalenko, S.I.; Babizhetskii, V.S.; Hartl, H.; Kuzma, Yu.B. New YMo_3B_7 boride and its structure. *Crystallogr. Rep.* **1995**, *40*, 424-427.

(36) Salamakha, L.; Sologub, O.; Rizzoli, C.; Michor, H.; Gonçalves, A.P.; Rogl, P.; Bauer, E. Crystal structure and physical properties of UMo_3B_7. *Intermetallics* **2017**, *85*, 180–186.

(37) Felten, E.J. The preparation of aluminum diboride, AlB_2. *J. Am. Chem. Soc.* **1956**, *78*, 5977-5978.

(38) La Placa, S.; Post, B. The crystal structure of rhenium diboride. *Acta Crystallogr.* **1962**, *15*, 97-99.

(39) Lundström, T. The structure of Ru_2B_3 and $WB_{2.0}$ as determined by single-crystal diffractometry, and some notes on the W-B system. *Ark. Kemi* **1969**, *30*, 115-12.

(40) Frotscher, M.; Klein, W.; Bauer, J.; Fang, C.-M.; Halet, J.-F.; Senyshyn, A.; Baehtz, C.; Albert, B. M_2B_5 or M_2B_4? Reinvestigation of the Mo/B and W/B system. *Z. Anorg. Allg. Chem.* **2007**, *633*, 2626-2630.

(41) Frotscher, M.; Hölzel, M; Albert, B. Crystal structures of the metal diborides ReB_2, RuB_2, and OsB_2 from neutron powder diffraction. *Z. Anorg. Allg. Chem.* **2010**, *636*, 1783-1786.

(42) Kuz'ma, Yu.B.; Akselrud, L.G.; Chaban, N.F.; Bruskov, V.A. The crystal structure of $Pr_5Co_2B_6$. *Dopov. Akad. Nauk Ukr. RSR* Ser. B **1983**, *10*, 49-52.

(43) Parthé, E.; Chabot, B.; Crystal Structures and Crystal Chemistry of Ternary Rare Earth-Transition Metal Borides, Silicides and Homologues in: Handbook on the Physics and Chemistry of Rare Earths, Eds. Gschneidner, K. Jr.; Eyring, L.; Elsevier, Amsterdam, **1984**, Vol. 6, ch. 48, 113-334; Salamakha, P.S.; Sologub, O.L.; Rizzoli, C.; Hester, J.R.; Stepien-Damm, J.; Gonçalves, A.P.; Lopes, E.B.; Almeida, M. Ternary RPt_4B (R=La, Ce, Pr, Nd) compounds; structural and physical characterisation. *Intermetallics* **2004**, *12*, 1325-1334. Salamakha, P.; Sologub, O.; Gonçalves, A.P.; Almeida, M. $Ce_2Ir_5B_2$, a new structure type of ternary borides. *J. Alloys Comp.* **2003**, *360*, 131–136. Sologub, O.L.; Salamakha, L.P.; Noel, H.; Roisnel, T.; Gonçalves A. $La_3Ru_8B_6$ and $Y_3Os_8B_6$, new members of a homologous series $RE(An)_nM_{3n-1}B_{2n}$. *J. Solid State Chem.* **2007**, *180*, 2740-2746; Salamakha, L.; Bauer, E.; Hilscher, G.; Michor, H.; Sologub, O.; Rogl, P.; Giester G. Structural and physical properties diversity of new $CaCu_5$-type related europium platinum borides. *Inorg. Chem.* **2013**, *52*, 4185-4197. Jung, W. $A_nRh_{3n-1}B_{2n}$ mit A = Ca und Sr, Eine Homologe Reihe Ternaerer Erdalkali-Rhodiumboride aus Bauelementen der $CeCo_3B_2$- und der $CaRh_2B_2$-Struktur. *J. Less-Common Met.* **1984**, *97*, 253-263.

(44) Quentmeier, D.; Jung, W. The crystal structure of $Ba_2Ni_9B_6$. *Z. Kristallogr.* **1980**, *151*, 172-174.

(45) Mirgel, R.; Jung, W. The ternary alkali metal platinum borides $LiPt_3B$, $NaPt_3B_{1+x}$ and $Na_3Pt_9B_5$ - new structure variants of the $CeCo_3B_2$ type. *J. Less-Common Met.* **1988**, *144*, 87-99.

(46) Filinchuk, Ya.E.; Yvon, K. Boron-induced hydrogen localization in the novel metal hydride $LaNi_3BH_x$ (x=2.5-3.0). *Inorg. Chem.* **2005**, *44(12)*, 4398-4406.

(47) Higashi, I.; Shishido, T.; Takei, H.; Kobayashi, T. Crystal structure of $PrRh_{4.8}B_2$. *J. Less-Common Met.* **1988**, *139*, 211-220.

(48) Kuz'ma, Yu.B. Crystal chemistry of borides, Vyshcha Shkola Press, Lvov, **1983**.

(49) Shi, Y.; Leithe-Jasper, A.; Tanaka, T. New ternary compounds $Sc_3B_{0.75}C_3$, $Sc_2B_{1.1}C_{3.2}$, $ScB_{15}C_{1.60}$ and subsolidus phase relations in the Sc-B-C system at 1700 C. *J. Solid State Chem.* **1999**, *148*, 250-259.

(50) Levchenko, G.; Lyashchenko, A.; Baumer, V.; Evdokimova, A.; Filippov, V.; Paderno, Yu.; Shitsevalova, N. Preparation and some properties of ScB_2 single crystals. *J. Solid State Chem.* **2006**,*179*, 2949–2953.

(51) Rogl, P.; Schuster, J. Phase diagrams of ternary boron nitride and silicon nitride systems, in *Monograph Series on Alloy Phase Diagrams*, ASM International: Materials Park, OH, USA, 1992.

(52) Frotscher, M.; Senyshyn, A; Albert, B. Neutron diffraction at metal borides, Ru_2B_3 and Os_2B_3. *Z. Anorg. Allg. Chem.* **2012**, *638*, 2078–2080.

(53) Aronsson, B.; Stenberg, E.; Aselius, J. Borides of ruthenium, osmium and iridium. Nature **1962**, *195*, 377-378.

(54) Kempter, C.P.; Fries, R.J. Crystallography of the Ru-B and Os-B Systems. *J. Chem. Phys*. **1961**, *34(6)*, 1994-1995.

(55) Mikhalenko, S.I.; Zavalii, L.V.; Kuz'ma, Yu.B.; Boiko, L.I. Isothermal sintering of the Sc-W-B and Sc-Re-B systems at 1000 °C. *Sov. Powder Metall.* **1991**, *30*, 681-683.

(56) Mykhalenko, S; Babizhetskyj, V; Kuz'ma, Yu. New compound in the system Sc-Cr-B. *J. Solid State Chem.* **2004**, *177*, 439-443.

(57) Chaban, N. F.; Mykhailenko, S. I.; Davydov, V. M.; Kuz'ma, Yu. B. Phase equilibria diagram of Lu–V–B system. *Powder Metall. Met. Ceram.* **2002**, *41***,** 162-168.

(58) Kotzott, D. Synthese und Charakterisierung von neuen und bekannten Hartstoffen und die technische Relevanz von Härteangaben. Inaugural-Dissertation, Universität Freiburg im Breisgau, **2009**.

(59) Horvath, C.; Rogl, P. New ternary borides with $LuRuB_2$-type. *Mater. Res. Bull*. **1985**, *20,* 1273-1278.

(60) Pasturel, A.; Colinet, C.; Hichter, P. Strong chemical interactions in disordered alloys. *Physica B* **1985**, *132*, 177-180.

(61) Jarlborg, T.; Freeman, A.J.; Watson-Yang, T.J. Electronic structure and reentrant magnetism in superconducting $ErRh_4B_4$. *Phys. Rev. Lett.* **1977**, *39(16)*, 1032-1034.

(62) Mott, N.F. The electrical conductivity of transition metals. *Proc. R. Soc.* **1936**, *153*, 699-717.

(63) Mott, N.F.; Jones, H. The theory of the properties of metals and alloys, Oxford Univ. Press, London, 1958.

Table of Contents Synopsis

Re-examination of the Sc-Ru-B system revealed two novel borides, $ScRu_2B_3$ and Sc_2RuB_6. While the size and shape of boron aggregation in Sc_2RuB_6 correlate well with the atomic percentage of boron and metal exhibiting planar nets of condensed boron pentagons, hexagons and heptagons, $ScRu_2B_3$ is an exception in the classification scheme of borides. It exhibits an unusual unique structure where the infinite $B6^3$ nets intercalate with $CeCo_3B_2$-related slabs. Excellent agreement between structural, physical and electronic structure characteristics has been achieved.

Table of Contents Graphic